

Measurement and Modeling of Creep in Open-Cell NiAl Foams

ANDREA M. HODGE and DAVID C. DUNAND

Nickel-rich NiAl foams, consisting of open cells with hollow struts and exhibiting two relative densities (5.0 and 6.6 pct) and average cell sizes (1.27 and 0.85 mm), were creep tested between 800 °C and 1100 °C under compressive stresses between 0.10 and 1.50 MPa. For stresses lower than 0.50 MPa, the foams exhibit secondary creep with power-law behavior characterized by creep exponents and activation energies close to those of bulk, nickel-rich NiAl. A three-dimensional (3-D) finite-element model (FEM) was implemented for a cell consisting of hollow struts on a cubic lattice, which predicts creep rates in reasonable agreement with the experimental data. Based on these numerical results, a simplified analytical model is proposed, whereby struts parallel to the applied stress deform by creep in a purely compressive mode, while perpendicular struts prevent buckling but provide no direct load-bearing capacity. This simple model produces results that are very close to the predictions of the complex numerical model and in good agreement with the experimental data. By contrast, an existing model considering creep bending of struts within the foam predicts strain rates that are too high by approximately two orders of magnitude.

I. INTRODUCTION

TO date, research on the mechanical behavior of cellular metals has mainly been focused on the room-temperature behavior of aluminum-based open- and closed-cell foams, as reviewed in References 1 through 4. Only a few reports exist on the high-temperature mechanical behavior of metal foams, which examine exclusively aluminum foams.^{15,6,7} A simple analytical model based on creep bending of struts within the foam was developed by Gibson and Ashby¹¹ and was found to be in general agreement with creep data for open-cell alumina foams (with a 10 to 21 pct relative density, between 1300 °C and 1500 °C¹⁸), for aluminum foams with open cells (relative density of 6 to 14 pct, tested between 275 °C and 350 °C¹⁵), and with closed cells (relative density of 8.7 pct, tested between 260 °C and 350 °C⁶). These studies show that, at low stresses, metallic foams exhibit the same creep exponent and activation energy as the bulk metal, as predicted theoretically by the strut creep-bending model of Gibson and Ashby.¹¹ At high stresses, anomalously high stress exponents have been measured in closed-cell aluminum foams crept at 300 °C^{6,7} and are linked to localized high-stress regions (crush bands) where the material exhibits power-law breakdown.¹⁷

Recently, we have developed a new process for the synthesis of nickel aluminide foams, based on pack aluminization of pure nickel foams.^{19,10} Homogenization at elevated temperatures resulted in foams with a single, homogenous NiAl phase, which retained the open-cell architecture and hollow struts of

the original nickel foams. These NiAl foams are expected to exhibit excellent oxidation and creep resistance up to approximately 1100 °C, with possible use as cores of sandwiches used for filters, heat exchangers, or load-bearing structures. While they are weaker than ceramic foams used at elevated temperatures,¹⁸ NiAl foams should be ductile above the ductile-to-brittle transition temperature (DBTT) of NiAl (280 °C to 730 °C¹¹) and exhibit much higher thermal conductivity and thermal shock resistance. Also, creating sandwich structures should be simpler for NiAl foams than for ceramic foams.

In the present article, we present creep results for NiAl foams tested between 800 °C and 1100 °C and compare them to predictions of the analytical model based on strut creep bending.¹¹ We also develop an idealized three-dimensional (3-D) finite-element model (FEM) to predict creep properties of the NiAl foams and carry out a parametric exploration of the effect of temperature, stress, foam density, and strut structure (hollow *vs* solid strut). These results lead to the development of a simple analytical model assuming pure compressive creep deformation of the foam struts.

II. EXPERIMENTAL PROCEDURES

Two unalloyed nickel foams (>99.0 pct purity) were procured from Astro Met (Cincinnati, OH) with 20 and 30 pores per linear inch (ppi), corresponding to average cell sizes of 1.27 and 0.85 mm. These foams consist of hollow struts connecting at joints to form an open-cell structure. The foam relative densities (ratio of foam density to solid density) and geometric parameters (cell size, strut width, and strut wall thickness) are listed in Table I. Foam density was calculated from mass and volume measurements, and the cell geometric parameters were determined from scanning electron microscope (SEM) micrographs. Electrodischarge machining was used to create parallelepiped specimens with the following dimensions: 10 × 10 × 22 mm and 12.7 × 12.7 × 25.4 mm.

ANDREA M. HODGE, formerly Graduate Student, Department of Materials Science and Engineering, Northwestern University, is Postdoctoral Fellow, Chemistry and Materials Science Department, Lawrence Livermore National Laboratory, Livermore, CA 94551. DAVID C. DUNAND, Professor, is with the Department of Materials Science and Engineering, Northwestern University, Evanston, IL 60208. Contact e-mail: dunand@northwestern.edu

Manuscript submitted November 21, 2002.

Table I. Geometric Parameters of As-Received Ni Foams and Aluminized NiAl Foams

Pores per Linear Inch (ppi)*	Cell Diameter (mm)**	Strut Width (μm)		Strut Wall Thickness (μm)		Relative Density (Pct)	
		Ni	NiAl [†]	Ni	NiAl [†]	Ni	NiAl
20	1.27	224 \pm 34	334	84 \pm 21	139	2.2	5.1
30	0.85	117 \pm 21	175	41 \pm 7	70	2.8	6.6

*Data from supplier.

**Calculated from the pores per linear inch value.

[†]Calculated from relative density increase.

NiAl foams were fabricated by pack aluminization of the machined nickel foam specimens, using an aluminization process similar to that presented in previous articles.^{19,101} Modifications were implemented to ensure that aluminum deposition was uniform over the whole volume of the specimens. The following modified pack composition was used: 3 wt pct NH_4Cl activator, 15 wt pct Al-Ni Raney-type powder (with 50 wt pct Al, from Alfa Aesar, Ward Hill, MA) and 82 wt pct Al_2O_3 powder. The sample and pack (40 g for the smaller samples and 45 g for the larger) were contained within a stainless steel bag. The bag was placed in a furnace under flowing argon, heated for 1 hour to the aluminization temperature of 1000 °C, held at that temperature for 4 hours (for the 30 ppi foams) or 1.5 hours (for the 20 ppi foams) and, subsequently, furnace cooled in 5 hours. The samples were then placed in a new pack and subjected to an additional aluminization treatment of 20 hours (for the 30 ppi foams) or 40 hours (for the 20 ppi foams). The pack was determined to be exhausted after about 4 hours, so the majority of the time for the second heat treatment was for homogenization of the concentration gradient produced during aluminization.^{19,101}

Creep tests were performed in air under constant compressive load, using a compression creep tester (Applied Test Systems) with SiC pushrods and an alumina spring enclosure to counteract the weight of the upper rod. The enclosure also prevented premature loading of the sample during heating and subsequent brittle damage below the DBTT of the foams. A linear voltage-displacement transducer (which was calibrated before each experiment) was attached at the cold end of a longitudinal extensometer transmitting the relative displacement of the pushrods. The furnace was brought to within ± 2.5 °C of the test temperature and equilibrated for over 1 hour before any loading occurred. Test temperatures spanned the range from 800 °C to 1100 °C, corresponding to homologous temperatures of 0.56 to 0.72 (using $T_m = 1638$ °C as the melting point of stoichiometric NiAl). At a given temperature, specimens were subjected to a series of increasing load values, yielding up to four strain-rate measurements, with no more than 10 pct strain accumulated in each specimen.

III. RESULTS

The processing times listed previously were found to yield optimal compositional and microstructural homogeneity (at the levels of struts and of the bulk samples), based on a metallographic investigation of samples processed at incrementally

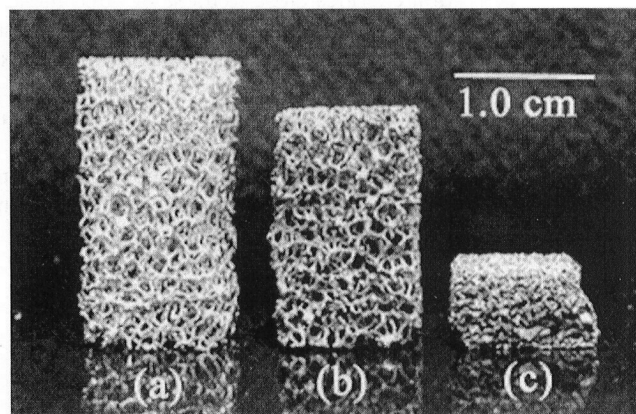


Fig. 1—20 ppi NiAl foam (a) as-processed, (b) deformed by approximately 20 pct at 0.8 MPa at 900 °C, and (c) deformed by approximately 70 pct at 1.5 MPa at 900 °C.

longer times. After the second aluminization/homogenization treatment, the struts consisted of single-phase, nickel-rich NiAl with an average composition, as measured by mass gain, of 70.4 wt pct Ni (52.0 at. pct Ni) for the 20 ppi foams (19 specimens), and 71.3 wt pct Ni (53.5 at. pct Ni) for the 30 ppi foams (nine specimens). The average composition from chemical analysis for both foams was 72.5 wt pct Ni (55 at. pct Ni). This value is expected to be more accurate, since mass-gain measurements are systematically skewed toward higher aluminum concentrations: small amounts of pack material attached to the foams, which could not be removed during ultrasonic cleaning, were measured as Al mass gain. The average NiAl grain size for both the 20 and 30 ppi foams was 40 ± 2 μm , using the line-intercept method and assuming a square grain shape. After aluminization, the average relative density of the foams was $\rho^* = 5.1$ pct for the 20 ppi foams and $\rho^* = 6.6$ pct for the 30 ppi foams. As described in more detail in References 9 and 10, the cell size and macroscopic dimensions of the specimens did not change upon aluminization (Figure 1(a)), but the strut diameter increased to accommodate the aluminum mass gain.

Figures 1(b) and (c) show 20 ppi NiAl foams deformed at relatively high stresses of 0.8 and 1.5 MPa, which resulted in instantaneous plastic deformation by yield at 900 °C. At this temperature, the NiAl foams were highly ductile, showing total plastic strains of approximately 20 and 70 pct, respectively. As illustrated in Figure 1(b), deformation to strains less than approximately 20 pct was macroscopically homogeneous, without localized compression crush bands observed in some Al foams.^{15,61}

Experimental strain vs time creep curves at 900 °C under stresses of 0.25, 0.35, and 0.45 MPa are shown in Figure 2 for a 20 ppi foam with $\rho^* = 5.5$ pct. The overall shape of the creep curves is similar to that of bulk NiAl and shows a primary region with decreasing strain rate, followed by a secondary regime where the strain rate reaches a minimum. This minimum strain rate was measured when the slope of the creep curve was constant within experimental error. For some samples, further creep measurements were performed at higher stresses at the same temperature. Table II lists all creep results performed on a subset of samples with average nickel compositions and relative densities, respectively, of $c_{Ni} = 70.4$ wt pct and $\rho^* = 5.0$ pct for the 20 ppi foams (ten specimens), or $c_{Ni} = 69.6$ wt pct

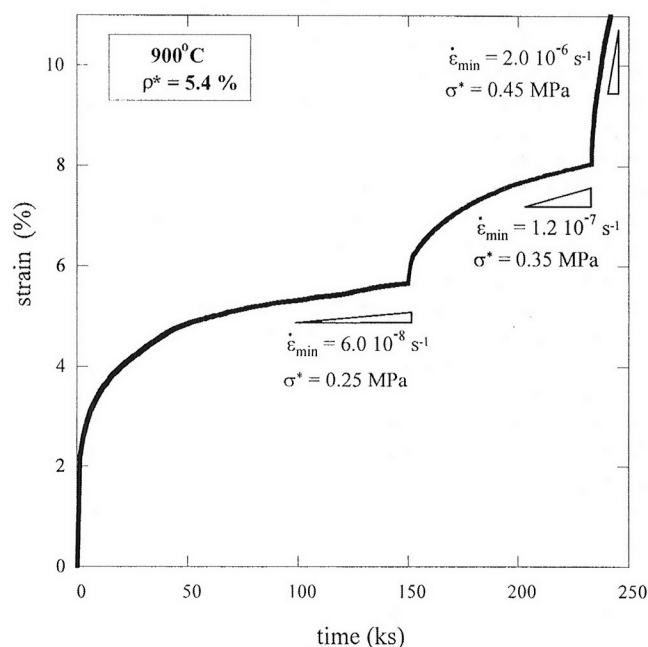


Fig. 2—Experimental compressive strain vs time curves for a 20 ppi foam, with a composition of 71.2 wt pct Ni and a relative density of $\rho^* = 5.5$ pct, crept at 900 °C at three different compressive stresses.

and $\rho^* = 6.6$ pct for the 30 ppi foams (two specimens). In Table II, the foam stress (σ^*) is given as the applied load divided by the cross-sectional area of the specimen (100 or 161 mm²); the stress within the foam struts is substantially higher, as described in Section IV.C.

Figure 3 is a logarithmic plot of minimum strain rate vs stress for a subset of 20 and 30 ppi foams tested at 900 °C.

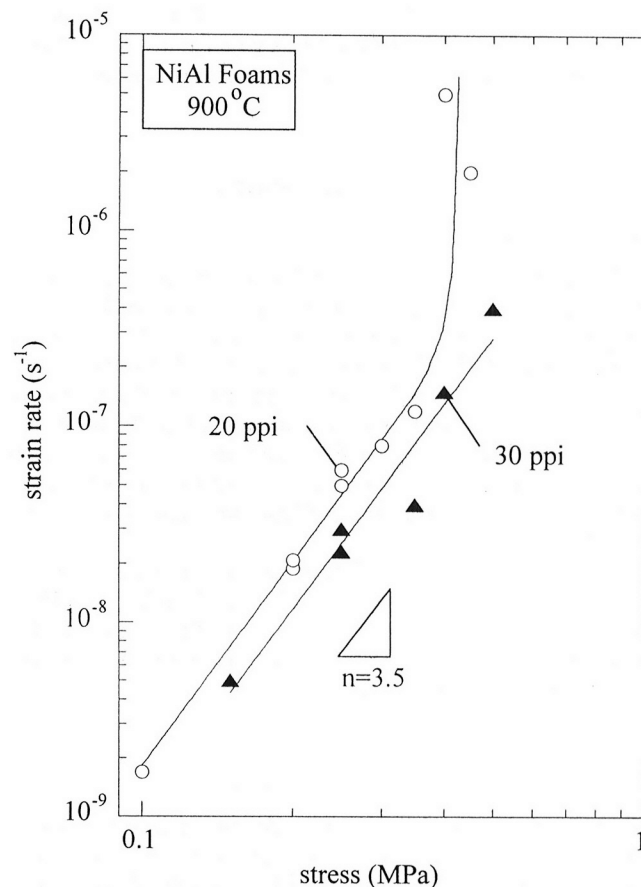


Fig. 3—Compressive strain rate vs compressive stress for 20 ppi foams ($\rho^* = 5.0$ to 5.5 pct) and 30 ppi foams ($\rho^* = 6.6$ pct) at 900 °C.

Table II. Creep Test Results for NiAl Foams

Temperature (°C)	Stress (MPa), Minimum Strain Rate (s ⁻¹)				Ni Content (Wt Pct)	Relative Density (Pct)
20 ppi foams						
800	0.15, 2.9 × 10 ⁻⁹				70.2	4.9
827	0.25, 1.4 × 10 ⁻⁸	0.40, 6.0 × 10 ⁻⁸			71.1	5.3
900	0.30, 2.2 × 10 ⁻⁷	0.40, 6.0 × 10 ⁻⁶			70.0	4.5
900	0.10, 1.7 × 10 ⁻⁹	0.20, 1.9 × 10 ⁻⁸	0.30, 8.0 × 10 ⁻⁸	0.40, 5.0 × 10 ⁻⁶	70.0	5.1
900	0.20, 2.1 × 10 ⁻⁸	0.25, 5.0 × 10 ⁻⁸			70.6	5.0
900	0.25, 6.0 × 10 ⁻⁸	0.35, 1.2 × 10 ⁻⁷	0.45, 2.0 × 10 ⁻⁶		71.2	5.5
1000	0.10, 6.3 × 10 ⁻⁹	0.25, 9.5 × 10 ⁻⁸	0.30, 3.0 × 10 ⁻⁷		70.9	5.1
1050	0.12, 9.0 × 10 ⁻⁸	0.22, 1.0 × 10 ⁻⁶			69.7	4.8
1100	0.15, 7.0 × 10 ⁻⁷				70.5	4.9
1100	0.12, 1.0 × 10 ⁻⁷				70.0	4.8
30 ppi foams						
900	0.15, 5.0 × 10 ⁻⁹	0.25, 3.0 × 10 ⁻⁸	0.35, 4.0 × 10 ⁻⁸		69.6	6.6
900	0.25, 2.3 × 10 ⁻⁸	0.40, 1.5 × 10 ⁻⁷	0.50, 4.0 × 10 ⁻⁷		69.6	6.6

Within experimental error, the creep-stress exponents (slopes of linear data in Figure 3) are identical for both foams ($n = 3.5$). The 30 ppi foam ($\rho^* = 6.6$) deforms at half the rate of the 20 ppi foam ($\rho^* = 5.0$ to 5.5 pct), as expected from their higher relative density. Power-law breakdown ($n \geq 7$) was observed above 0.35 MPa for the 20 ppi foams, but was not displayed by the 30 ppi foams up to the highest measured stress of 0.5 MPa, again due to their higher density. Finally, the effect of oxidation was studied by holding 20 ppi foams in air at 900 °C for 360 hours, at 1000 °C for 168 hours, and at 1100 °C for 120 hours. Mass gains at the end of these experiments were 3.5, 1.6, and 1.5 pct, respectively.

IV. DISCUSSION

A. Microstructure

The factor R , by which the relative density of the foams increases after aluminization (assuming no change in macroscopic dimensions), can be calculated as $R = 2.30$ for stoichiometric NiAl,¹⁹ in good agreement with present experimental values of $R = 2.31$ and 2.35 for the 20 and 30 ppi foams, respectively. The strut diameter (D) and wall thickness (t) can then be estimated,¹⁹ assuming that all mass gain during aluminization is accommodated by an increase in outside diameter of the struts. These dimensions are shown in Table I.

The mass gains recorded after long-term exposure of the foams in air at 900 °C to 1100 °C are expected to originate in the native alumina layer growing on the surface of the struts. An estimate of the oxide layer thickness (Δt) is found by simple geometric considerations as

$$\Delta t = t \frac{\Delta m}{m} \frac{\rho_{\text{NiAl}}}{\rho_{\text{Al}_2\text{O}_3}} \quad [1]$$

where t is the strut-wall thickness, $\Delta m/m$ is the foam relative mass gain, and the densities are $\rho_{\text{NiAl}} = 5.65 \text{ g/cm}^3$ and $\rho_{\text{Al}_2\text{O}_3} = 3.97 \text{ g/cm}^3$. Using $t = 139 \text{ }\mu\text{m}$ for the 20 ppi foams (Table I), the oxide thickness given by Eq. [1] is 7 μm for the foam with the highest mass gain in Table II (exposed for 15 days at 900 °C). Most foams tested in the present study are expected to exhibit oxide surface layers on the order of 1 to 2 μm , which is much thinner than the strut-wall thickness of $t = 139$ and 70 μm . This oxide layer is likely to crack without significantly strengthening the foams at the relatively rapid creep rates measured in the present study. For NiAl foams with higher surface-to-volume ratios, strengthening by the native oxide layer may, however, become significant at very slow strain rates and very long exposure times.

B. High-Stress Deformation Mechanisms

For ductile metallic foams, creep can occur in a stable manner only at stresses below the compressive yield stress (σ_y^*) at which plastic collapse occurs. For open-cell foams, assuming formation of plastic hinges at the strut joints, the following equation can be derived for the foam yield stress:^[1]

$$\sigma_y^* \approx 0.3 \sigma_y \rho^{*3/2} \quad [2]$$

where σ_y is the yield strength of the bulk material, and ρ^* is the relative density of the foam. Equation [2] was found to predict within a factor of approximately 2 the yield stress of aluminum foams at ambient temperature with relative densities in the range of 3 to 40 pct.^[3] Using an approximate value of $\sigma_y = 100 \text{ MPa}$ for nickel-rich NiAl at 900 °C,^[11] Eq. [2] predicts a foam yield stress of $\sigma_y^* \approx 0.35$ and 0.51 MPa for the 20 and 30 ppi foams, respectively. As illustrated in Figures 1 and 3, the experimental yield stress at 900 °C is above 0.45 MPa but below 0.80 MPa for the 20 ppi foams and above 0.50 MPa for the 30 ppi foams, in general agreement with the previous estimation. We do not attempt to quantify elastic buckling^[1] or creep buckling,^[12] because the values for the materials' imperfection parameters, needed for these models, are unknown.

At stresses just below the yield stress, breakdown of the power-law regime was observed for the 20 ppi foams at stresses of 0.40 and 0.45 MPa (Figure 3). A similar breakdown region at high stresses was observed in alumina foams crept at 1300 °C to 1500 °C^[8] and in aluminum foams crept at 275 °C to 300 °C.^[16,7] The latter authors correlated this behavior to steplike collapse of individual cell layers leading to crush bands where the material is heavily deformed. In our experiments, however, no such steplike collapse was observed, as large-scale deformation occurred in a macroscopically homogeneous manner (as illustrated in Figure 1(b)), resulting in a smooth creep curve (Figures 2(a) through (c)). It is, however, likely that yield or power-law breakdown is occurring locally throughout the foam in the high-stress region of Figure 3, resulting in the nonlinear behavior visible in that figure. Our tests were performed to total strains less than 10 pct, so it is possible that steplike collapse through crush bands may occur at higher strains.

C. Finite-Element Modeling of Creep

Two-dimensional (2-D) and 3-D FEMs have been developed to describe elasticity and time-independent plasticity of foams in, *e.g.*, References 13 through 17. For creep of metallic foams, however, very few FEM studies exist: several 2-D models^[5,18–20] and, very recently, a 3-D Voronoi model.^[21] We use here a 3-D FEM using the ABAQUS software (Pawtucket, RI). The unit cell consists of three orthogonal sets of four parallel hollow or solid struts with square cross section, connecting at joints arranged on a square lattice (Figure 4). The geometric parameters of the models are summarized in Table III. Two relative densities (5.0 and 5.5 pct) are considered for both types of struts (hollow and solid). The actual architecture of the NiAl foams (Figure 1(a)) is much less regular than the simple cubic lattice shown in Figure 4; the model is, thus, a simplified representation of the general geometry of the NiAl foam, but it captures some of their important features such as hollow struts and 3-D periodicity.

Periodic boundary conditions are implemented by creating constraint equations, setting the degrees of freedom of boundary nodes equal to each other on the eight vertical faces of each of the two sets of four horizontal struts (directions 2 and 3 in Figure 4). The FEM nodes at the bottom surface of the four vertical struts are completely

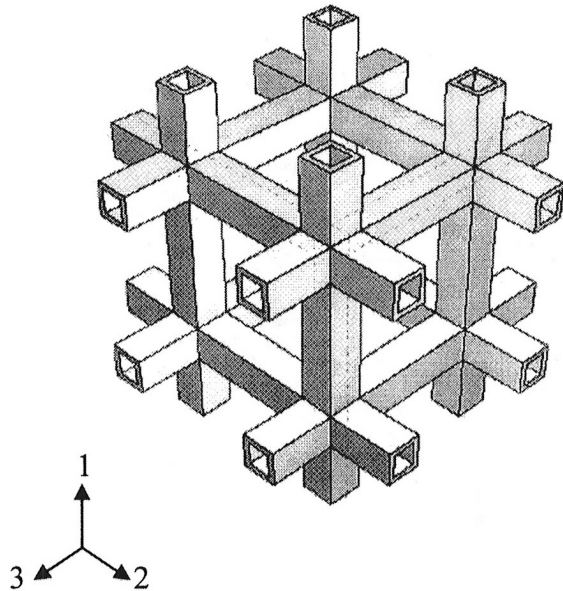


Fig. 4—Geometric FEM models for foam with hollow struts ($\rho^* = 5.0$ pct). In the solid-strut model, struts have smaller width but the same cross sectional area.

Table III. Geometric Parameters for FEM Cell

Relative Density (Pct)	Cell Diameter* (μm)	Strut Width (μm)	Strut Wall Thickness (μm)
5.0	1090	130.0	solid
5.5	1106	138.0	solid
5.0	1253	211.6	30.8
5.5	1253	211.6	34.1

*Edge-to-edge distance.

fixed. The periodic boundary conditions simulate an infinite 3-D array of cells connected to each other. Loading is performed in the vertical 1 direction, in the form of a distributed load on the cross-sectional areas of the four vertical struts; the displacement of these nodes is then used to calculate the strain of the cell. Creep of the NiAl material within the struts and joints is assumed to take place according to the power-law equation, where the steady-state strain rate $\dot{\epsilon}$ is related to the uniaxial applied stress σ as follows:

$$\dot{\epsilon} = A\sigma^n \exp\left(\frac{-Q}{RT}\right) \quad [3]$$

where A is the Dorn constant, n is the stress exponent, Q is the activation energy, R is the gas constant, and T is the temperature. The bulk creep parameters n and K ($K = A \exp(-Q/RT)$) are determined from Yang and Dodd's study for Ni-rich NiAl^[22] and are listed in Table IV, together with the Young's modulus (E) and Poisson's ratio (ν) from References 11 and 23, which are also needed as input in the model. As compared to the only other 3-D FEM of creep in metallic foams,^[21] the present model exhibits a large number of elements for a single regular cell with

Table IV. Creep^[22] and Elastic^[11,23] Parameters for Ni-45 At. Pct Al Used in FEM Calculations

T ($^{\circ}\text{C}$)	K ($\text{MPa}^{-n}\text{s}^{-1}$)	n (—)	E (GPa)	ν (—)
800	1×10^{-13}	3.6	161	0.33
900	3×10^{-12}	3.4	157	0.33
1000	7×10^{-12}	3.8	153	0.33
1100	4×10^{-10} *	3.2*	149	0.33

*Extrapolated.

periodic conditions, while the Voronoi model of Reference 21 considers a large number of irregularly shaped cells (also with periodic conditions), but with only four elements for each strut.

Figures 5(a) and (b) show typical strain vs time creep curves calculated at 900 $^{\circ}\text{C}$ for applied stresses of $\sigma^* = 0.1$ and 0.6 MPa, spanning the experimental range of stresses at that temperature. Two curves are shown for foams with a 5.5 pct relative density and with solid or hollow struts. At the lowest stress, a noticeable primary-creep region occurs, followed by a secondary stage for which the minimum strain-rate value was taken when the rate was changing by less than 1 pct over a period of 2 to 4 hours, depending on the length of the FEM simulation. The primary creep visible in Figures 5(a) and (b) is not due to primary creep in NiAl, as deformation was assumed to take place solely by secondary, power-law creep (Eq. [3]). It may represent artifacts of the FEM convergences, as also observed by Andrews and Gibson.^[24] Given that the model is very idealized as compared to the true foam structure, this small error was neglected. Comparing the minimum strain rates for the two different geometries at a 5.5 pct relative density, the hollow-strut structure deforms faster than the solid-strut structure at the lower stress of 0.1 MPa (Figure 5(a)), but slightly slower at the highest stress of 0.6 MPa (Figure 5(b)).

The lower stress sensitivity of the hollow-strut structure is also visible in Figures 6(a) and (b), where the minimum strain rate is plotted as a function of stress for both densities (5.0 and 5.5 pct) and both geometries (hollow and solid struts): the apparent stress exponent is $n = 3.0$ for the hollow-strut structure and $n = 3.4$ for the solid-strut structure. It is also visible from Figures 6(a) and (b) that foams with the higher density of 5.5 pct are predicted to deform at a slower rate than those with the lower density of 5.0 pct foams, as expected qualitatively. Also plotted in Figures 6(a) and (b) are the experimental creep results for NiAl foams with relative densities between 5.0 and 5.5 pct, for which the stress exponent is $n = 3.5$. The agreement between the FEM calculations and the experimental data is surprisingly good (less than a factor-of-2 difference in creep rate), given the simplifications used in the geometric model. The predicted creep rates are always lower than the experimental data, as expected from the fact that the applied load is assumed to be parallel to the struts of the FEM cell, which is the strongest direction of the cell. In the actual NiAl foam, most struts were subjected to a multiaxial state of stress and deformed by creep under a combination of compression and bending at a higher rate than pure, uniaxial compression, which is the dominant deformation mechanism in the vertical

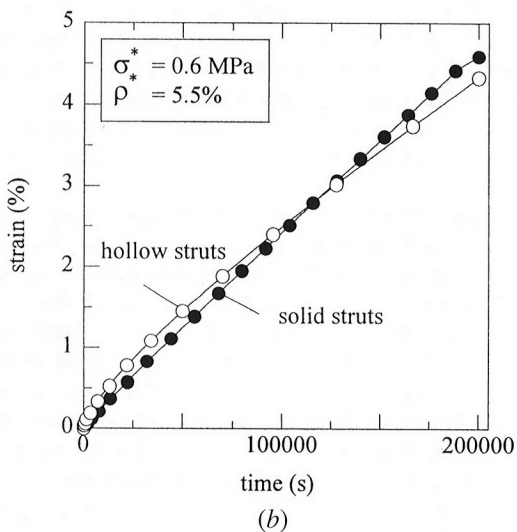
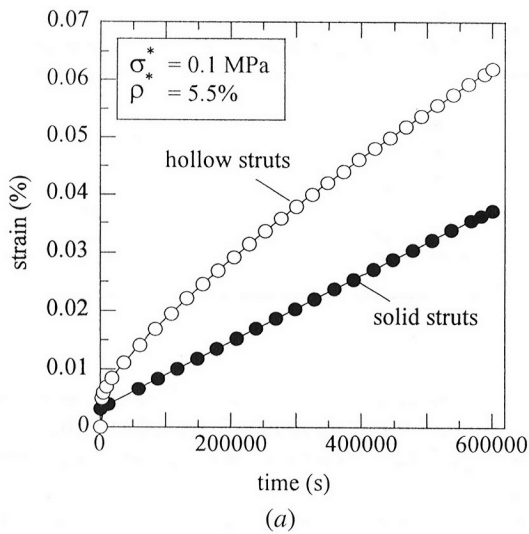


Fig. 5—Compressive strain vs time curves calculated by FEM at 900 °C for foams with hollow and solid struts ($\rho^* = 5.5$ pct) at stresses (a) $\sigma^* = 0.1$ MPa and (b) $\sigma^* = 0.6$ MPa.

struts of the FEM structure. Also, the struts in the experimental NiAl foams exhibit curvature, variation in cross section, and defects, all of which increase the foam creep rate.^[21]

The apparent-stress exponent at 900 °C for the solid-strut structures is $n = 3.4$, equal to the stress exponent of bulk, nickel-rich NiAl (Table IV) used as an input parameter in the calculations. This is expected, as creep deformation takes place mostly in the vertical struts parallel to the uniaxial applied stress, with the horizontal struts (normal to the applied stress) carrying very little stress and only preventing buckling of the vertical struts. The distribution of Von Mises stresses, shown in Figure 7(a) for a foam deformed under a stress of 0.2 MPa at 900 °C in the minimum-strain-rate regime, indeed shows that the stress in the vertical struts is uniform and high, except in the immediate vicinity of the joints, where the horizontal struts are locally reducing the stress within the vertical struts. One strut diameter away from the joint, the Von Mises

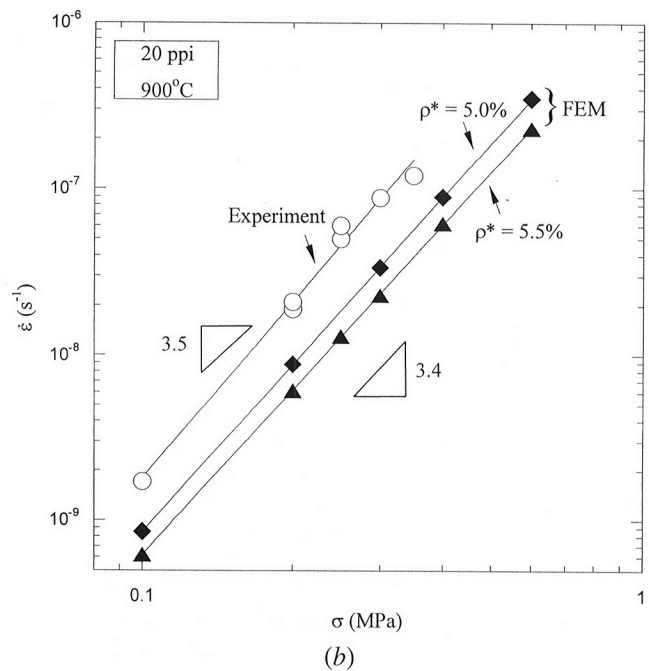
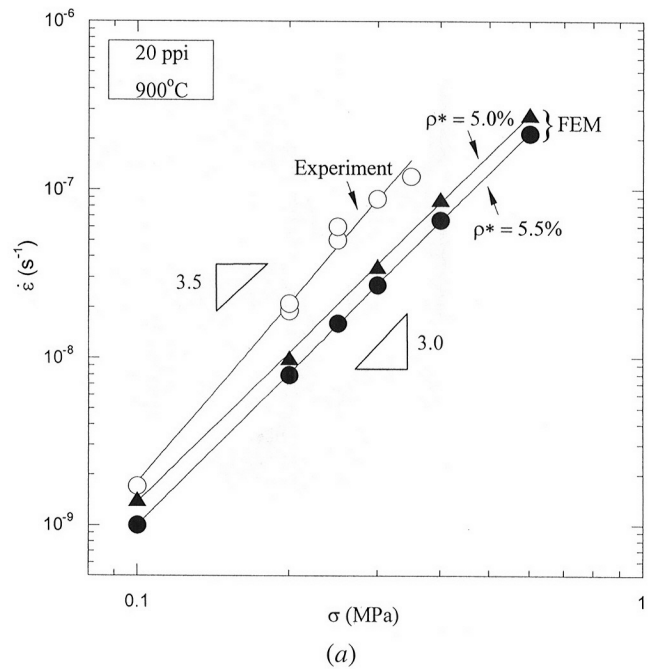


Fig. 6—Compressive strain rate vs stress curves at 900 °C as measured experimentally on 20 ppi foams ($\rho^* = 5.0$ to 5.5 pct) and as calculated by FEM ($\rho^* = 5.0$ and 5.5 pct) for (a) hollow struts and (b) solid struts.

stress averaged over the whole volume of the horizontal struts is, however, insignificant as compared to the stress within the vertical struts.

The stress state in the hollow-strut structure is more complex. At low applied stresses, the higher creep rate of the hollow-strut model (Figure 5(a)) can be explained by weakening at the joints, where the hollow struts intersect. The joints exhibit six square holes from the struts, which weaken their load-bearing capability. This is visible in Figure 7(b), showing that the highest value of the Von Mises

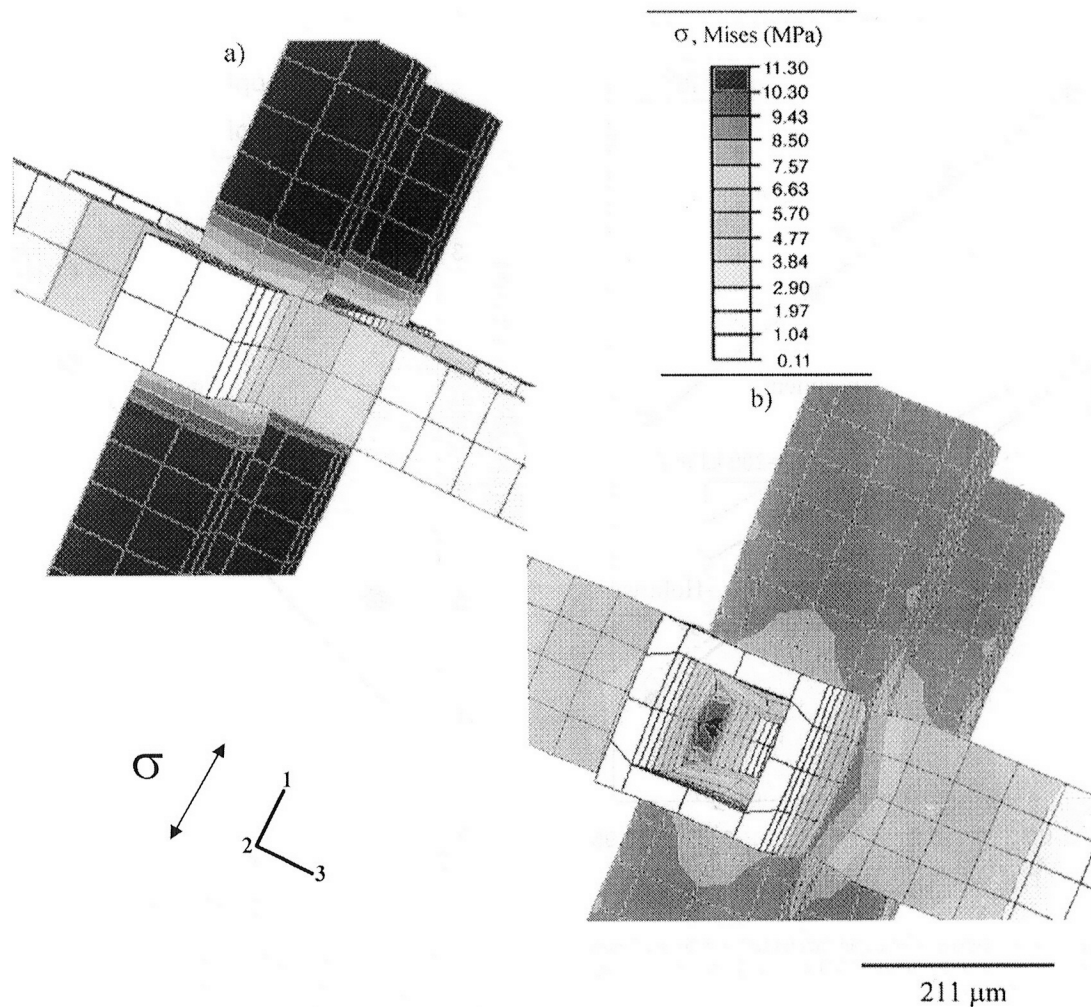


Fig. 7—Von Mises effective stress for an external stress $\sigma^* = 0.2$ MPa at 900 °C after achieving minimum strain rate for foams ($\rho^* = 5.5$) with (a) solid struts and (b) hollow struts. Uniaxial compressive loading is parallel to the 1 direction.

stress is within the hollow joint, near the region where the hollow struts converge. However, the hollow horizontal struts carry comparatively more stress than their solid counterparts (Figure 7(a)), thus partially unloading the vertical struts and slowing the overall creep rate. This effect becomes dominant at higher stress, thus reducing the creep rate of the hollow-strut model as compared to the solid-strut model (Figure 5(b)). This leads to an apparent stress exponent of $n = 3.0$, below the input value for bulk NiAl ($n = 3.4$). However, for the range of stresses and temperatures studied, the difference in creep rate between the hollow- and solid-strut models is small (Figures 6(a) and (b)). If the struts were deforming mostly by creep bending (e.g., if the applied stress was not parallel to the struts), the cell with hollow struts would be expected to be more creep resistant than a cell with solid struts, based on the higher bending strength of tubes as compared to solid bars of the same mass.

Figure 8 shows an Arrhenius plot of the temperature dependence of FEM creep rates at a constant stress ($\sigma^* = 0.25$ MPa). As in Figures 6(a) and (b), the FEM creep rates are quite close to the experimental data. The slopes of the lines in Figure 8 represent the apparent

activation energies, which take a value of 210 and 272 kJ/mol for the FEM hollow- and solid-strut models, respectively. The apparent activation energy for the solid-cell model is the same as the average value determined from Yang and Dodd's study^[22] for Ni-rich NiAl ($Q = 272$ kJ/mol) used as input in the model, as expected if uniaxial compressive creep of the vertical struts is responsible for most of the deformation. However, for the hollow-strut structure, the value of Q is significantly lower than the input value for NiAl, an effect similar to the decrease in the apparent stress exponent to $n = 3.0$ (Figures 6(a) and (b)) from the input NiAl value of $n = 3.4$. The larger contribution from the horizontal struts to the overall foam creep strength is probably responsible for both effects. The experimental foam creep data in Figure 8 (for $\sigma = 0.22$ to 0.25 MPa and $\rho^* = 5.0$ to 5.5 pct) provide $Q = 200$ kJ/mol, in agreement with the value of $Q = 195 \pm 19$ kJ/mol found by regression of all experimental data (as described in Section D). However, given the substantial experimental errors and uncertainties in Q values for nickel-rich NiAl, the differences in Q values between the data and models are probably not significant.

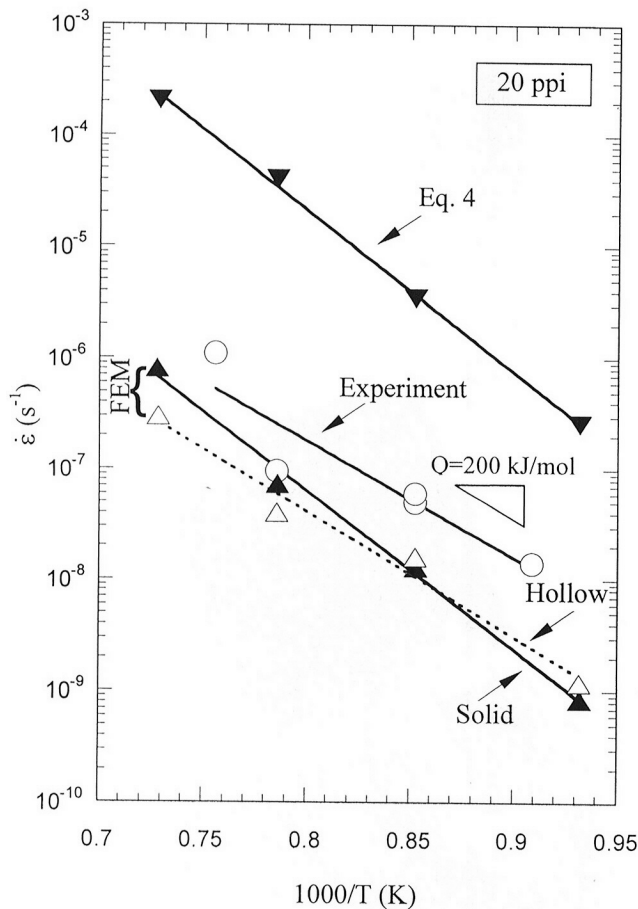


Fig. 8—Arrhenius plot of creep data for experimental tests on 20 ppi foams ($\rho^* = 5.0$ to 5.5 pct, $\sigma^* = 0.22$ to 0.25 MPa) and FEM predictions ($\rho^* = 5.5$ pct, $\sigma^* = 0.25$ MPa).

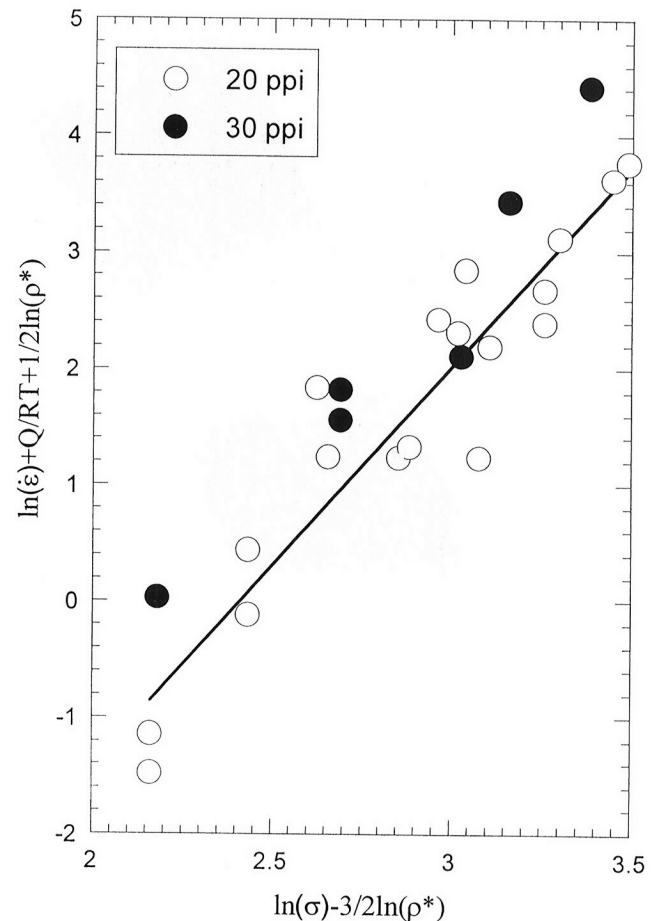


Fig. 9—Compressive creep data for 20 ppi foams ($\rho^* = 4.5$ to 5.5 pct) and 30 ppi foams ($\rho^* = 6.6$ pct) between 800 °C and 1100 °C, plotted according to Eq. [4].

D. Analytical Modeling of Creep

Gibson and Ashby^[1] considered a unit cell where joints consist of two horizontal struts and one vertical strut. The vertically applied load is transmitted through each vertical strut (assumed rigid) and results in the deformation of the two corresponding horizontal struts by creep bending. Based on this cell geometry, these authors developed an equation for the macroscopic strain rate ($\dot{\epsilon}^*$) of the cell (or, equivalently, of the foam) as

$$\dot{\epsilon}^* = A \frac{0.6}{n+2} \left(\frac{1.7(2n+1)}{n} \right)^n \sigma^{*n} \rho^{*-(3n+1)/2} \exp\left(\frac{-Q}{RT}\right) \quad [4]$$

where σ^* is the foam stress. Equation [4] can be rewritten in logarithmic form as

$$\ln \dot{\epsilon}^* = \ln B - \frac{1}{2} \ln \rho^* + n(\ln \sigma^* - \frac{3}{2} \ln \rho^*) - \frac{Q}{RT} \quad [5]$$

where B is the product of the first three terms in the right-hand side of Eq. [4]. Using all experimental data listed in Table II (except those in the high-stress, breakdown region), a linear-regression analysis using least-squares fit yielded values for the two unknowns: $n = 3.4 \pm 0.3$ and

$Q = 195 \pm 19$ kJ/mol. The fit is illustrated in Figure 9, which contains all power-law creep data measured between 800 °C and 1100 °C, for stresses between 0.10 and 0.50 MPa and for relative densities between 4.8 and 6.6 pct.

Figures 7(a) and (b) indicate that, to a good approximation, the uniaxial deformation of the cell is given by the average creep rate of the four vertical struts, representing one-third of the cell volume (or slightly more, if the whole joint volume is considered to be load bearing). Then, the creep rate of a cell with relative density of ρ^* can be approximated by the creep rate of a cell with relative density of $\rho^*/3$ containing only vertical struts. The creep equation for the foam becomes

$$\dot{\epsilon}^* = A \left(\frac{\rho^*}{3} \right)^{-n} \sigma^{*n} \exp\left(\frac{-Q}{RT}\right) \quad [6]$$

and is independent of whether the struts are hollow or solid. The previous equation assumes pure creep compression of the vertical struts, unlike Eq. [4], which considers pure creep bending of the horizontal struts. Using all the experimental power-law data listed in Table II, a linear-regression analysis of Eq. [6] gave values of $n = 3.4 \pm 0.3$ and $Q = 206 \pm 18$ kJ/mol, with a slightly better fit than that for Eq. [4]: $R^2 = 0.909$ vs $R^2 = 0.892$.

For bulk NiAl, the stress exponent and the activation energy for creep can vary significantly, depending on stoichiometry, grain size, impurities, and fabrication routes: $n = 3.5$ to 10 and $Q = 215$ to 310 kJ/mol.^[11,25] Only the study by Yang and Dodd^[22] examined in detail the creep of NiAl with a composition (55 at. pct or 72.6 wt pct Ni) close to those of the present foams (Table II). They reported a stress exponent varying between 3.4 and 3.8 between 800 °C and 1000 °C (Table IV), in good agreement with the previous values ($n = 3.4 \pm 0.3$). Performing a regression analysis on the creep data of Yang and Dodd^[22] for stresses of 40 to 70 MPa and temperatures of 800 °C to 1000 °C results in a Dorn exponent of $A = 12.4$ MPa⁻ⁿs⁻¹, a stress exponent of $n = 3.24 \pm 0.23$, and a creep activation energy of 276 ± 8 kJ/mol. The latter value is higher than those determined for the NiAl foams using Eqs. [4] and [6] ($Q = 195$ to 206 ± 19 kJ/mol), but this discrepancy may be due to the hollow nature of the struts, as illustrated in Figure 8, where $Q = 200$ kJ/mol was obtained for the FEM structure with hollow struts.

Both models (Eqs. [4] and [6]) predict, after linear regression of the data, the same apparent stress exponents and activation energies, within statistical error. By contrast, the magnitude of the creep rates predicted by the models differ by approximately two orders of magnitude, as illustrated in Figure 10 at 900 °C, using creep data in Table IV. The creep-compression model (Eq. [6]) predicts creep rates which are too low by a factor of 2, as compared to the experimental data, and which are also very close to the FEM predictions (shown in Figure 6). On the other hand, the creep-bending model (Eq. [4]) overpredicts the experimental creep rates by a factor of over 100; that model was also found to overestimate by a factor of approximately 8 the creep rate of open-cell aluminum foams measured at 275 °C.^[5] It must be taken into consideration that the hollow-strut geometry

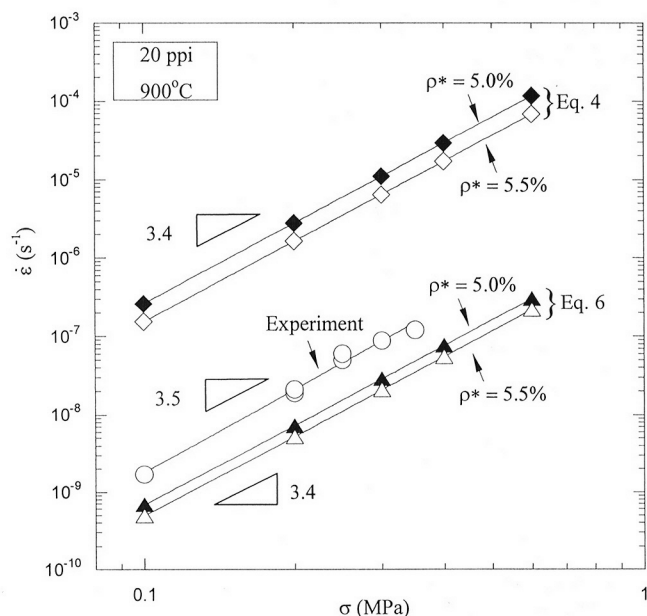


Fig. 10—Compressive strain rate vs stress plot at 900 °C showing experimental data for 20 ppi foams ($\rho^* = 5.0$ to 5.5 pct) and predictions of analytical models assuming creep bending of struts (Eq. [4]) or creep compression of struts (Eq. [6]) for $\rho^* = 5.0$ and 5.5 pct.

does not affect the predictions of the creep-bending model appreciably, given the high ratio of wall thickness to strut diameter, as shown by Goretta *et al.*^[8] Figure 11 shows a comparison of the predictions of the two models (Eqs. [4] and [6]) with experimental data at all temperatures and foam densities. We conclude that, for the present NiAl foams at the temperature and stress ranges studied, the complex deformation taking place within the struts (which gives rise to the steady-state creep rate measured experimentally on the foam) is quite accurately estimated by considering uniaxial creep compression of struts (Eq. [6]), but is significantly overpredicted when considering pure creep bending of struts (Eq. [4]).

The two models represent extreme cases for the deformation of open-cell foams with different joint geometries (illustrated in the inset of Figure 12). The present model (Eq. [6]) assumes joints where six struts converge, thus allowing compressive deformation of the struts as the main deformation mode, while the model by Ashby and Gibson (Eq. [4]) assumes three struts at each joint, permitting only bending deformation. The model predictions diverge with decreasing foam density, as depicted in Figure 12, where the ratio of the strain rates predicted by Eqs. [4] and [6] varies with $\rho^{*-n/2}$. This figure illustrates that the difference

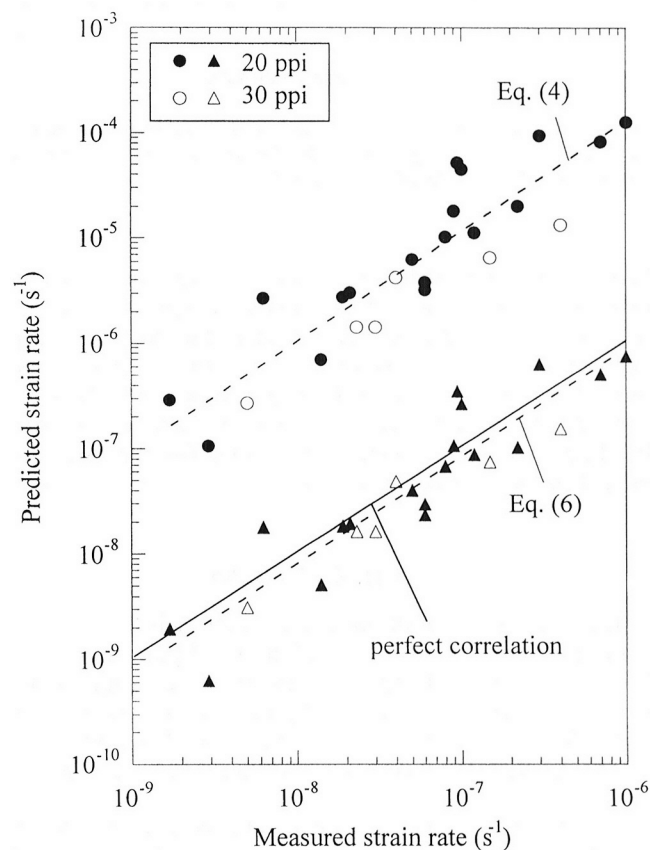


Fig. 11—Comparison between experimentally measured creep rates (for 20 and 30 ppi foams between 800 °C and 1100 °C) plotted on the x -axis and creep rates predicted from analytical models plotted on the y -axis (1) assuming creep bending of struts (Eq. [4]), circles show a discrepancy by a factor of approximately 100 from perfect correlation and (2) creep compression of struts (Eq. [6]), triangles show a discrepancy by a factor approximately 2). Dotted lines are best-fit regressions.

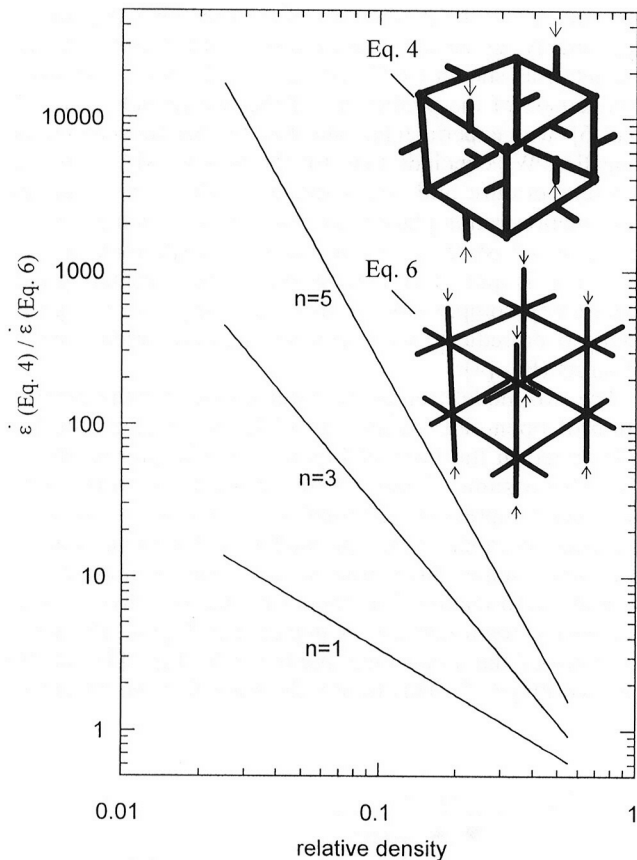


Fig. 12—Ratio of foam strain rates predicted with the creep-bending model (Eq. [4]) and the creep-compression model (Eq. [6]), as a function of relative density; the ratio is independent of temperature.

between the two models becomes very substantial at low relative densities for a stress exponent typical of metals ($n = 3$ to 5). The discrepancy is reduced for the lower creep exponents usually exhibited by ceramics ($n = 1$ to 3). Thus, the details of the foam architecture, especially the strut connectivity, which controls the relative amounts of strut bending and compression, are crucial for the accurate prediction of the creep of foams.

V. CONCLUSIONS

The creep behavior of open-cell, nickel-rich NiAl foams, exhibiting cells measuring 1.27 mm (20 ppi, density of 5.1 pct) or 0.85 mm (30 ppi, density of 6.6 pct) with hollow struts, was measured for compressive stresses of $\sigma = 0.1$ to 0.5 MPa over a temperature range of $T = 800$ °C to 1100 °C. The following conclusions have been reached.

1. The apparent creep exponent and activation energy calculated by linear regression are $n = 3.4 \pm 0.3$ and $Q = 195 \pm 19$ kJ/mol. These values are comparable to those reported for bulk nickel-rich NiAl ($n = 3.2 \pm 0.2$ and $Q = 276 \pm 8$ kJ/mol).
2. Power-law breakdown ($n \geq 7$) was observed above 0.35 MPa for the 20 ppi foams and was not observed for 30 ppi foams up to 0.5 MPa, because of their higher

average relative density. Steplike collapse of cells, reported in Al foams, was not observed.

3. A 3-D FEM was used to simulate the creep behavior of a NiAl foam consisting of cubic cells with solid or hollow struts. The FEM creep-rate predictions are slower by a factor of 2 as compared to experimental data. Predictions are modestly sensitive to foam density and strut geometry (hollow vs solid).
4. The FEM creep exponents ($n = 3.0$ to 3.4) are close to the value used for bulk NiAl in the model and are near the experimental results ($n = 3.4 \pm 0.3$). The FEM activation energy for $\sigma = 0.25$ MPa is 272 kJ/mol for a solid-strut structure and 210 kJ/mol for a hollow-strut structure, in good agreement with the experimental result of 195 ± 19 kJ/mol.
5. The analytical model for foam creep by Gibson and Ashby^[1] (Eq. [4]), which assumes creep bending of struts as the main deformation mechanism, overestimates the experimental foam creep rate by approximately two orders of magnitude.
6. A simple analytical model (Eq. [6]), which considers creep compression of the struts, provides predictions very close to those produced by FEM and within a factor of 2 of the experimental creep data.
7. The connectivity of struts at the joints should determine which analytical model is better suited: if few struts converge into joints, the strut creep-bending model (Eq. [4]) should be applicable; if the joints consist of many struts, the present strut creep-compression model (Eq. [6]) may be more appropriate.

ACKNOWLEDGMENTS

This research was supported by NASA through Grant No. NCC3-870. One of the authors (AMH) acknowledges the support of the Zonta Foundation in the form of the Amelia Earhart Fellowship. The authors thank Drs. M.V. Nathal and J.D. Whittenberger for useful discussions and use of experimental facilities during two visits by AMH to the NASA Glenn Research Center.

REFERENCES

1. L.J. Gibson and M.F. Ashby: *Cellular Solids: Structures and Properties*, 1st ed., Cambridge University Press, Cambridge, United Kingdom, 1988.
2. L.J. Gibson and M.F. Ashby: *Cellular Solids: Structures and Properties*, 2nd ed., Cambridge University Press, Cambridge, United Kingdom, 1997.
3. L.J. Gibson: *Ann. Rev. Mater. Sci.*, 2000, vol. 30, pp. 191-227.
4. M.F. Ashby, A. Evans, N.A. Fleck, L.G. Gibson, J.W. Hutchinson, and H.N.G. Wadley: *Metals Foams: A Design Guide*, Butterworth Heinemann, Boston, MA, 2000.
5. E.W. Andrews, L.J. Gibson, and M.F. Ashby: *Acta Mater.*, 1999, vol. 47, pp. 2853-63.
6. E.W. Andrews, J.-S. Huang, and L.J. Gibson: *Acta Mater.*, 1999, vol. 47, pp. 2927-35.
7. P. Zhang, M. Haag, O. Kraft, A. Wanner, and E. Arzt: *Phil. Mag. A*, 2002, vol. 82, pp. 2895-907.
8. K.C. Goretta, R. Brenzy, C.Q. Dam, D.J. Green, A.R. De Arellano-Lopez, and A. Dominguez-Rodriguez: *Mater. Sci. Eng.*, 1990, vol. 124A, pp. 151-58.
9. A.M. Hodge and D.C. Dunand: *Intermetallics*, 2001, vol. 9, pp. 581-89.

10. D.C. Dunand, A.M. Hodge, and C. Schuh: *Mater. Sci. Technol.*, 2002, vol. 18, pp. 326-32.
11. R.D. Noebe, R.R. Bowman, and M.V. Nathal: *Int. Mater. Rev.*, 1993, vol. 38, pp. 193-232.
12. A.C.F. Cocks and M.F. Ashby: *Acta Metall.*, 2000, vol. 48, pp. 3395-400.
13. A.E. Simone and L.J. Gibson: *Acta Mater.*, 1998, vol. 46, pp. 3929-35.
14. P.R. Onck, E.W. Andrews, and L.J. Gibson: *Int. J. Mech. Sci.*, 2001, vol. 43, pp. 681-99.
15. H.X. Zhu, J.F. Knott, and N.J. Mills: *J. Mech. Phys. Solids*, 1997, vol. 45, pp. 319-43.
16. A.P. Roberts and E.J. Garboczi: *J. Mech. Phys. Solids*, 2002, vol. 50, pp. 33-55.
17. A.G. Hanssen, O.S. Hopperstad, M. Langseth, and H. Ilstad: *Int. J. Mech. Sci.*, 2002, vol. 44, pp. 359-406.
18. H.X. Zhu, J.R. Hobdell, and A.H. Windle: *Acta Mater.*, 2000, vol. 48, pp. 4893-900.
19. E. Andrews, W. Sanders, and L.J. Gibson: *Mater. Sci. Eng.*, 1999, vol. 270A, pp. 113-24.
20. R.K. Oruganti and A.K. Ghosh: in *Processing and Properties of Lightweight Cellular Metals and Structures*, A.K. Ghosh, T. Sanders, and D. Claar, eds., TMS, Warrendale, PA, pp. 211-21.
21. J.S. Huang and L.J. Gibson: *Mater. Sci. Eng.*, 2003, vol. A339, pp. 220-26.
22. W.J. Yang and R.A. Dodd: *Met. Sci. J.*, 1973, vol. 7, pp. 41-47.
23. N. Rusovic and H. Warlimont: *Phys. Status Solidi*, 1979, vol. 53, pp. 283-88.
24. E.W. Andrews and L.J. Gibson: *Mater. Sci. Eng.*, 2001, vol. 303A, pp. 120-26.
25. D.B. Miracle: *Acta Metall. Mater.*, 1993, vol. 41, pp. 649-84.